Seasonal and long-term vertical deformation in the Nepal Himalaya constrained by GPS and GRACE measurements

Yuning Fu[1] and Jeffrey T. Freymueller[1]

Received 9 October 2011; revised 27 January 2012; accepted 30 January 2012; published 23 March 2012.

[1] We analyze continuous GPS measurements in Nepal, southern side of the Himalaya, and compare GPS results with GRACE observations in this area. We find both GPS and GRACE show significant seasonal variations. Further comparison indicates that the observed seasonal GPS height variation and GRACE-derived seasonal vertical displacement due to the changing hydrologic load exhibit very consistent results, for both amplitude and phase. For continuous GPS stations whose observation time span are longer than 3 years, the average WRMS reduction is ~45% when we subtract GRACE-derived vertical displacements from GPS observed time series. The comparison for annual amplitudes between GPS observed and GRACE-derived seasonal displacements also shows consistent correlation. The good seasonal correlation between GPS and GRACE is due to the improved GPS processing strategies and also because of the strong seasonal hydrological variations in Nepal. Besides the seasonal signal, GRACE also indicates a long-term mass loss in the Himalaya region, assuming no GIA effect. This mass loss therefore will lead to crustal uplift since the earth behaves as an elastic body. We model this effect and remove it from GPS observed vertical rates. With a 2D dislocation model, most GPS vertical rates, especially in the central part of Nepal, can be interpreted by interseismic strain from the Main Himalayan Thrust, and several exceptions may indicate the complexity of vertical motion in this region and some potential local effects.

Citation: Fu, Y., and J. T. Freymueller (2012), Seasonal and long-term vertical deformation in the Nepal Himalaya constrained by GPS and GRACE measurements, *J. Geophys. Res.*, *117*, B03407, doi:10.1029/2011JB008925.

1. Introduction

[2] Seasonal hydrospheric mass movements cause periodic displacements of the lithosphere. Global Positioning System (GPS) coordinate variations, principally for the vertical component, have been used to investigate global [*Blewitt et al.*, 2001; *Dong et al.*, 2002; *Wu et al.*, 2003] and local [*Grapenthin et al.*, 2006] seasonal deformation modes, and the relationship between seasonal load and strain within active tectonic areas [*Heki*, 2001; *Bettinelli et al.*, 2008]. With the development of satellite gravimetry, especially the Gravity Recovery and Climate Experiment (GRACE), the time-variable gravity field and mass variation from the surface water and ice, can be quantitatively estimated [*Chen et al.*, 2006; *Luthcke et al.*, 2008; *Bruinsma et al.*, 2010].

[3] The GRACE-derived time-variable gravity field coefficients can be converted to harmonic coefficients for crustal deformation in three components, E, N, H [*Kusche and Schrama*, 2005; *van Dam et al.*, 2007], which provides a way to quantitatively compare and correlate GRACE and GPS measurements. *Van Dam et al.* [2007] compared GPS observed heights over Europe with GRACE predicted heights, and found the annual signals for those two measurements did not show good agreement; this was thought to be due to spurious annual signals propagated during GPS processing. *Khan et al.* [2010] realized that the GRACE measurements in Greenland underestimated the uplifts for GPS stations, and attributed this difference to the varied spatial sensitivity of GPS and GRACE for changing loads. With better GPS processing strategies and improved correction models (atmosphere delay, atmosphere loading, etc.) applied, considerable global agreement between GPS and GRACE has been observed in the regions where hydrologic seasonal effects are significant and local effects are small [*Tregoning et al.*, 2009; *Tesmer et al.*, 2011].

[4] The Himalaya, as the planet's highest mountain range, was created by the collision between the Indian and Eurasian plates during the last 40 million years [*Molnar and Tapponnier*, 1975]. It also contains one of the largest collections of glaciers outside the Arctic and Antarctic, with glacier coverage area of 34,659.62 km^2 [*Thomas and Rai*, 2005]. Glaciers and snowpack in the Himalaya and Tibet feed the great Asian rivers and supply water to millions of people for living. Therefore, the Himalaya and Tibet are

[1]Geophysical Institute, University of Alaska Fairbanks, Fairbanks, Alaska, USA.

0148-0227/12/2011JB008925

Table 1. Information of GPS Stations[a]

Station	Latitude	Longitude	Observation Time	WRMS Reduction in Height/North/East (%)	GPS Vertical Rates (mm/yr)	GRACE-Derived Uplift (mm/yr)
BMCL[b]	28.655	81.714	2007.21–2010.93	35.91/40.38/−4.16	0.65 ± 0.73	1.26 ± 0.04
BRN2	26.519	87.272	2009.38–2009.85	N/A	N/A	0.82 ± 0.05
BRTG	26.438	87.281	2004.20–2008.92	N/A	−1.50 ± 0.79	0.82 ± 0.05
BYNA	29.474	81.200	2009.29–2010.29	42.74/39.40/−1.45	N/A	1.23 ± 0.04
CHLM[b]	28.207	85.314	2004.24–2010.91	52.12/48.00/6.65	4.60 ± 0.37	0.74 ± 0.04
DAMA[b]	27.608	85.107	1997.90–2010.26	43.28/41.89/2.66	2.16 ± 0.21	0.86 ± 0.05
DLPA[b]	28.983	82.817	2007.35–2010.90	50.75/23.29/−5.71	4.61 ± 0.55	0.94 ± 0.04
DNGD	28.754	80.581	2008.34–2010.73	36.69/14.10/5.56	1.08 ± 0.62	1.54 ± 0.05
DRCL	29.733	80.500	2008.20–2010.94	47.56/24.96/−1.50	3.87 ± 0.68	1.37 ± 0.04
GNTW	29.176	80.626	2008.32–2010.94	22.98/11.91/2.17	2.61 ± 1.23	1.45 ± 0.04
GRHI[b]	27.950	82.491	2007.34–2010.90	43.63/−14.83/−1.43	4.95 ± 0.58	1.20 ± 0.05
GUMB[b]	27.909	85.877	1997.90–2010.26	48.05/33.91/7.97	6.07 ± 0.21	0.76 ± 0.04
JMLA[b]	29.277	82.192	2007.37–2010.89	44.24/26.13/−0.57	3.10 ± 0.73	1.02 ± 0.04
JMSM[b]	28.805	83.743	2004.33–2010.90	50.23/24.16/12.51	3.79 ± 0.33	0.81 ± 0.04
KKN4[b]	27.800	85.278	2004.22–2010.74	49.33/37.04/−6.71	2.05 ± 0.29	0.82 ± 0.04
KLDN[b]	27.766	83.603	2004.28–2010.15	33.43/38.78/10.15	1.25 ± 0.21	1.03 ± 0.05
LHAS	29.657	91.104	1995.38–2007.07	31.36/26.19/8.79	0.62 ± 0.27	0.69 ± 0.04
LHAZ[b]	29.657	91.104	1999.92–2011.23	38.40/42.40/3.69	2.04 ± 0.17	0.69 ± 0.04
MST2	29.177	83.953	2009.81–2009.82	N/A	N/A	0.69 ± 0.04
MSTG	29.178	83.894	2004.32–2009.80	N/A	N/A	0.70 ± 0.04
NPGJ[b]	28.117	81.595	2007.38–2010.88	47.71/33.01/6.62	−2.14 ± 0.58	1.37 ± 0.05
ODRE[b]	26.866	87.392	2004.86–2010.16	54.43/24.51/7.14	−1.29 ± 0.35	0.81 ± 0.05
RBIT	26.849	89.392	2003.81–2005.99	37.42/8.28/4.08	N/A	0.78 ± 0.05
RMJT	27.305	86.550	2009.84–2009.84	N/A	N/A	0.80 ± 0.05
RMTE	26.990	86.597	2008.73–2010.15	55.36/25.44/20.06	2.19 ± 1.16	0.83 ± 0.05
SIM4[b]	27.165	84.985	2004.23–2010.26	51.92/32.06/0.64	−0.16 ± 0.33	0.93 ± 0.05
SIMR[b]	27.164	84.984	1997.91–2005.37	24.09/15.96/7.69	3.90 ± 0.48	0.93 ± 0.05
SMKT	29.969	81.806	2008.37–2010.89	45.76/12.16/10.41	5.38 ± 0.64	0.95 ± 0.04
SRNK	28.260	83.935	2005.28–2010.83	27.64/15.05/6.82	0.94 ± 0.42	0.89 ± 0.04
SYBC	27.814	86.712	2008.76–2009.89	54.20/48.96/−2.54	N/A	0.74 ± 0.04
TIMP[b]	27.471	89.634	2002.38–2008.26	45.60/41.69/−4.84	−1.92 ± 0.45	0.78 ± 0.05
TPLJ[b]	27.352	87.709	2004.19–2010.17	46.14/49.37/3.19	1.55 ± 0.32	0.77 ± 0.05

[a]N/A: the observation time span is too short or signals are too noisy.
[b]The sites used for the stack in Figures 4 and 10.

called the "Water Tower of Asia" [*Thomas and Rai*, 2005]. In addition, the seasonal hydrological cycle around the high mountains of the Himalaya is significant: during the summer season from June through September, the high Himalaya range blocks the northward moisture-rich monsoon winds, so that moist air is raised in altitude and cooled down in temperature; this results in strong precipitation, especially on the southern side of the range. Additionally, the annual cycle of accumulation and melt of mountain snow and ice contributes to the seasonal hydrological variations.

[5] In this study, we use two kinds of geodetic techniques, continuous GPS and GRACE, to study the seasonal mass change and its resulting vertical displacement in Nepal and southern Tibet. We also discuss the long-term mass loss revealed by GRACE measurements and its impacts on tectonic vertical rates evaluations.

2. Geodetic Measurements

2.1. Continuous GPS Observations and Data Analysis

[6] Caltech and other groups have installed ~30 continuous GPS stations in Nepal (Table 1), and some of them have continuous observations for more than one decade. These GPS data are publicly available through Caltech's Tectonics Observatory website and the UNAVCO archive. We used the GIPSY/OASIS II software (Version 5.0) to process the GPS data and estimate station coordinates for these stations and others in the surrounding area in point positioning mode. We adopted JPL's reanalysis orbit and clock products, which were determined using a consistent set of models over the entire time span, including absolute antenna phase center models for both GPS receiver and satellite antennas [*Schmid et al.*, 2007]. We used the GMF tropospheric mapping function [*Boehm et al.*, 2006], and adopted a priori dry tropospheric delay estimates from the Global Pressure and Temperature (GPT) model [*Boehm et al.*, 2007]. Ocean tide loading effects were corrected using ocean tide model TPXO7.0 with Greens Functions modeled in the reference frame of CM (center of the mass of the whole Earth system) to maintain consistency with JPL's orbit/clock products and therefore avoid systematic errors [*Fu et al.*, 2012]. Nontidal ocean variations and atmospheric loading are not removed in the daily GPS analysis, and their effects remain in the GPS time series along with deformation due to other load variations that have periods >1 day.

[7] In order to remove the effects of atmospheric loading on the GPS coordinates, we computed the displacements due to atmospheric loading using data and programs developed by the GGFC (Global Geophysical Fluid Center) (T. van Dam, NCEP Derived 6 hourly, global surface displacements at 2.5 × 2.5 degree spacing, http://geophy.uni.lu/ncep-loading.html, 2010), which utilized the NCEP (National Center of Environmental Protection) reanalysis surface pressure data set. The GRACE solutions adopted in this study have two

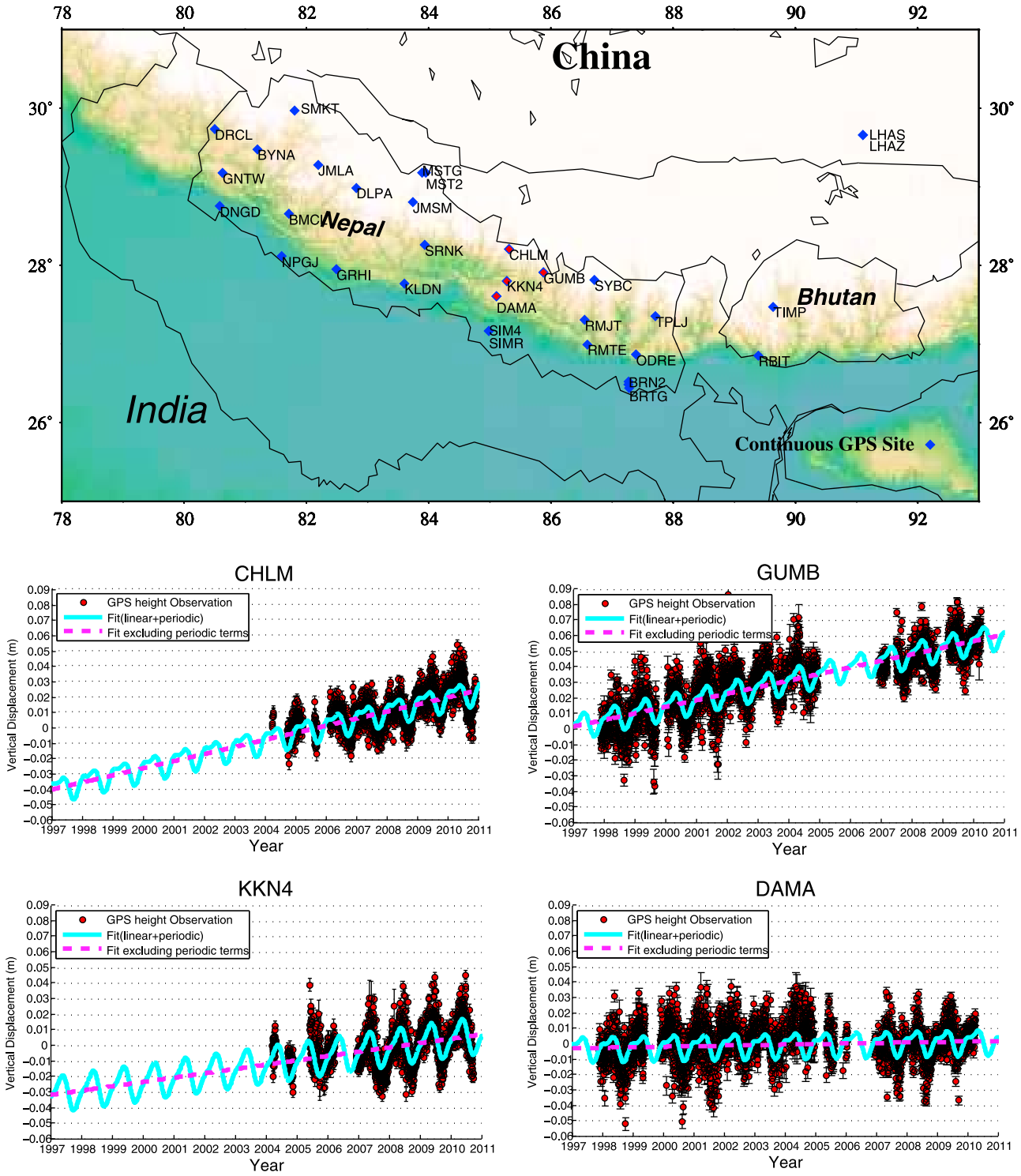

Figure 1. Locations of continuous GPS stations in Nepal, and example time series for sites CHLM, GUMB, KKN4 and DAMA (red diamonds in the location map). GUMB and DAMA have longer observational time than CHLM and KKN4.

different temporal resolutions: 10 days (GRGS) and a month (CSR, GFZ and JPL). We first derive the daily averaged atmospheric loading, and then average those daily results into 10 day and monthly corrections and remove them from 10 day and monthly averaged GPS solutions.

2.2. GRACE Models

[8] We employed the second release of 10 day gravity fields models (RL02) derived by the Space Geodesy Research Group (GRGS), in France. Spherical harmonic coefficients up to degree and order 50 for the gravity field

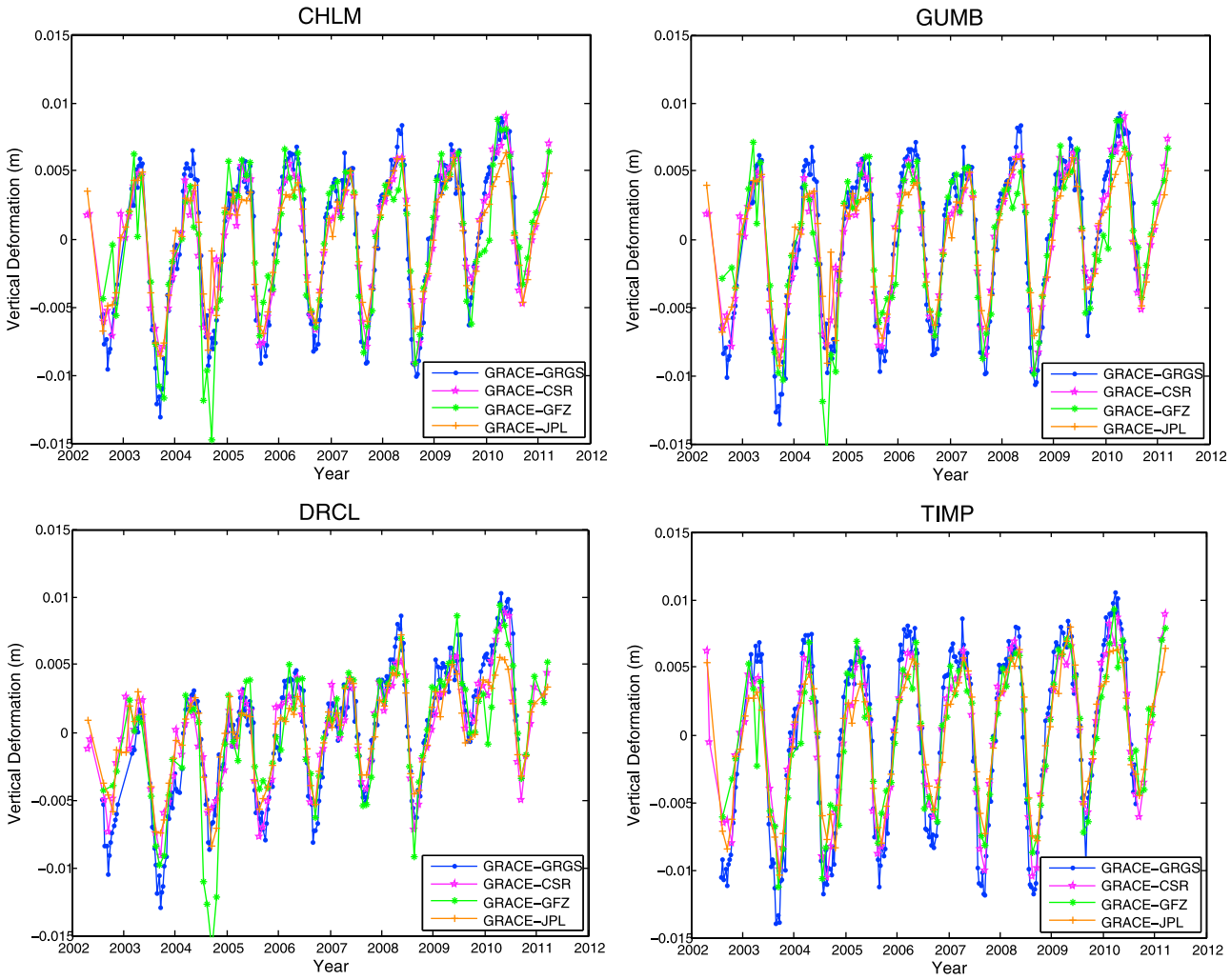

Figure 2. GRACE-derived vertical displacement time series due to the changing load calculated for four GPS stations, CHLM, GUMB, DRCL, TIMP. CHLM and GUMB are the same sites as shown in Figure 1. DRCL and TIMP are two more distant sites chosen for comparison. Results from different GRACE solution providers (GRGS, CSR, GFZ and JPL) are all presented.

are provided every 10 days. The details of the GRACE data processing can be found in the reference by *Bruinsma et al.* [2010]. No further smoothing or filtering is required for GRGS products, because they have been stabilized during their data analysis. Because LAGEOS observations are incorporated in the GRGS's gravity solutions, lower degrees, especially C20, are well constrained [*Bruinsma et al.*, 2010]. We replace the degree-1 components with results obtained by *Swenson et al.* [2008].

[9] We also compared GRACE Level-2 RL-04 solutions from several other groups: CSR (Center for Space Research, Austin, USA), GFZ (GeoForschungsZentrum, Potsdam, Germany), and JPL (Jet Propulsion Laboratory, USA). For those monthly products, we replace C20 terms with the results from observations of Satellite Laser Ranging [*Cheng and Tapley*, 2004], and Degree-1 terms using Stokes coefficients derived by *Swenson et al.* [2008]. For GRACE monthly solutions from CSR, GFZ and JPL, we adopted 400 km as the averaging radius to implement Gaussian smoothing, which suppresses errors at high degrees [*Wahr et al.*, 1998; *van Dam et al.*, 2007].

2.3. Displacements Due to the Changing Load

[10] Displacement in height due to the changing mass load can be expressed in terms of spherical harmonic coefficients for the gravity field and load Love numbers [*Kusche and Schrama*, 2005; *van Dam et al.*, 2007]

$$\Delta h(\theta,\phi) = R\sum_{l=1}^{\infty}\sum_{m=0}^{l}\overline{P}_{lm}(\cos\theta)\cdot\left[C_{lm}\cos(m\phi)+S_{lm}\sin(m\phi)\right]\cdot\frac{h_l'}{1+k_l'}, \quad (1)$$

in which R is the Earth radius; $\overline{P}_{lm}$ are fully normalized Legendre functions for degree l and order m; C_{lm} and S_{lm} are spherical harmonic coefficients of the gravity field, and h_l' and k_l' are Load Love numbers at degree l; we adopt Load Love numbers provided by *Farrell* [1972], which are computed in the center of mass of solid earth frame. Similar equations can be used to compute the horizontal displacements [e.g., *Kusche and Schrama*, 2005].

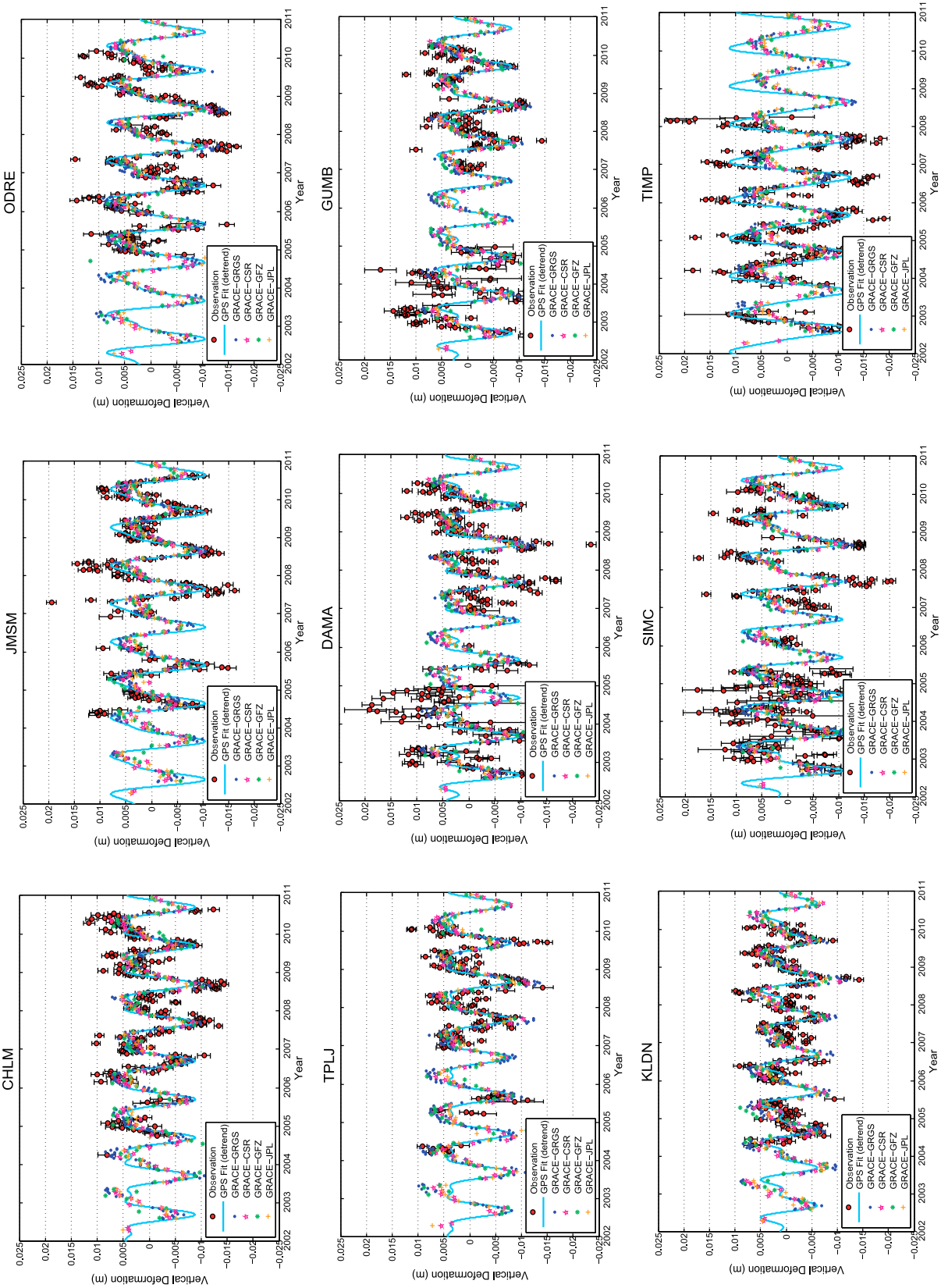

Figure 3. Comparison between 10 day averaged GPS detrended heights and GRACE-derived detrended seasonal vertical displacements. Red dots with error bar: 10 day averaged GPS observed detrended vertical deformation. Solid line: best fit (annual plus semi-annual components) for GPS detrended time series; GRACE solutions from four data centers are demonstrated with different colors. "SIMC" is a composite time series combining SIMR and SIM4.

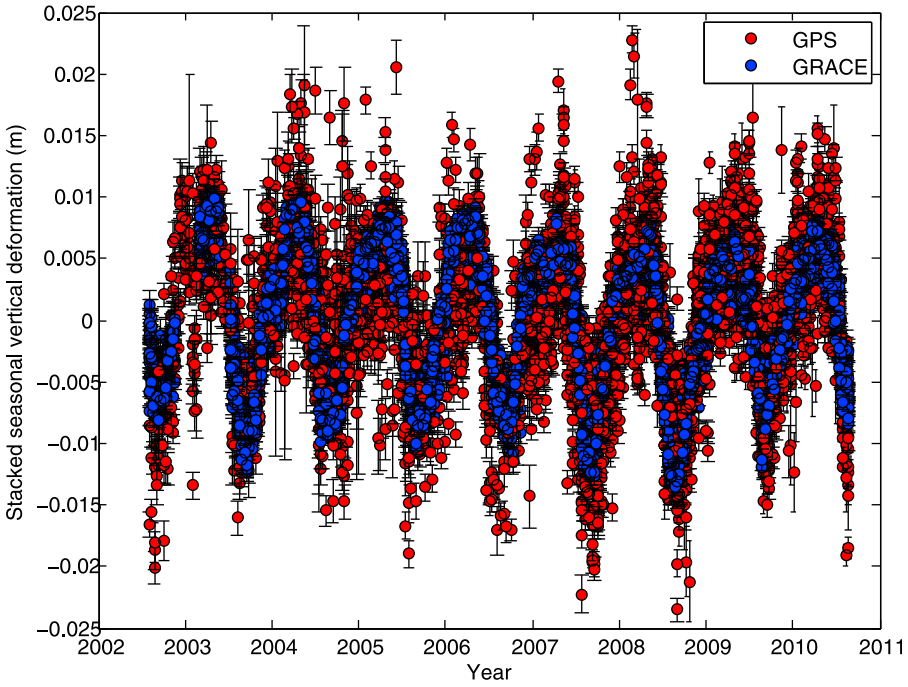

Figure 4. Stacked 10 day averaged GPS seasonal (detrended) vertical time series and GRACE-derived seasonal vertical time series, for the sites with data spans >3 years (see Table 1).

[11] We also tested loading computations with half-space models, and spherical earth models using cylindrical loads, with a load history based on GRACE mascon solutions. We found both of these computational methods to be problematic. The spatial extent of the load was too large for a half-space model, although the data could be fit well if the Young's modulus was increased as more distant loads were included in the computation. Using disk loads proved to be less computationally efficient than the Love number approach given that loads over a large region had to be considered.

3. Comparison Between GPS and GRACE-Derived Seasonal Height Variations

[12] Figure 1 shows the locations of continuous GPS stations in the Nepal Himalaya, and four example time series of daily solutions for GPS sites CHLM, GUMB, KKN4, DAMA. Besides the long-term linear trends, which are mainly dominated by tectonic processes, all GPS time series show significant seasonal variations. The peak-to-peak seasonal amplitude can be more than two centimeters, which reflects the strong seasonal hydrological fluctuations in Nepal. *Steckler et al.* [2010] studied similar seasonal phenomenon in Bangladesh with hydrographic, GPS and GRACE data. The average peak-to-peak vertical seasonal displacement in Bangladesh (5 $\sim$ 6 cm) are larger than those in Nepal (2 $\sim$ 4 cm), due to the very large seasonal river loading in Bangladesh.

[13] The vertical displacements are computed at the GPS sites from the GRACE-derived gravity field coefficients using equation (1), and four selected stations (CHLM, GUMB, DRCL, TIMP) are shown in Figure 2. CHLM and GUMB are the same sites whose GPS time series are shown in Figure 1. DRCL and TIMP are two more distant sites selected for comparison. Solutions from GRGS, CSR, GFZ and JPL exhibit very similar and consistent results, although there are several obvious outliers in 2004 for the GFZ solutions. In addition to the remarkable seasonal oscillations, a general uplift trend is also predicted. In this computation, we assume that the secular change in the gravity field is due to present day surface mass load changes [*Matsuo and Heki*, 2010], with no contribution from Glacial Isostatic Adjustment (GIA) or tectonic processes like crustal thickening (see section 5.2).

[14] In Figure 3, we compare the 10 day averaged detrended GPS height time series and GRACE-derived seasonal (detrended) vertical deformation due to the load change. GRACE solutions from GRGS, CSR, GFZ, JPL are all shown together. Results for nine example stations are plotted in Figure 3, in which "SIMC" is a composite time series combining two sites SIMR and SIM4 located 136.84 m apart. In all cases, there is a very close correspondence between the observed GPS and GRACE variations. To emphasize this, we choose a group of GPS stations based on the criteria that the observation span is longer than 3 years, and plot the stacked 10 day averaged GPS and GRACE-derived seasonal (detrended) vertical time series for these stations (Figure 4). The GPS and GRACE data clearly display very similar and consistent seasonal patterns for both magnitude and phase. For the remainder of this paper, we will use the average seasonal variations measured by GRACE, computed by fitting a model with a linear trend and annual and semiannual periodic terms, for comparison to the seasonal variations observed by GPS. The seasonal variations should come from the same physical cause (seasonal mass transport) for both height and gravity change, whereas the long-term trends of the two measurements are expected

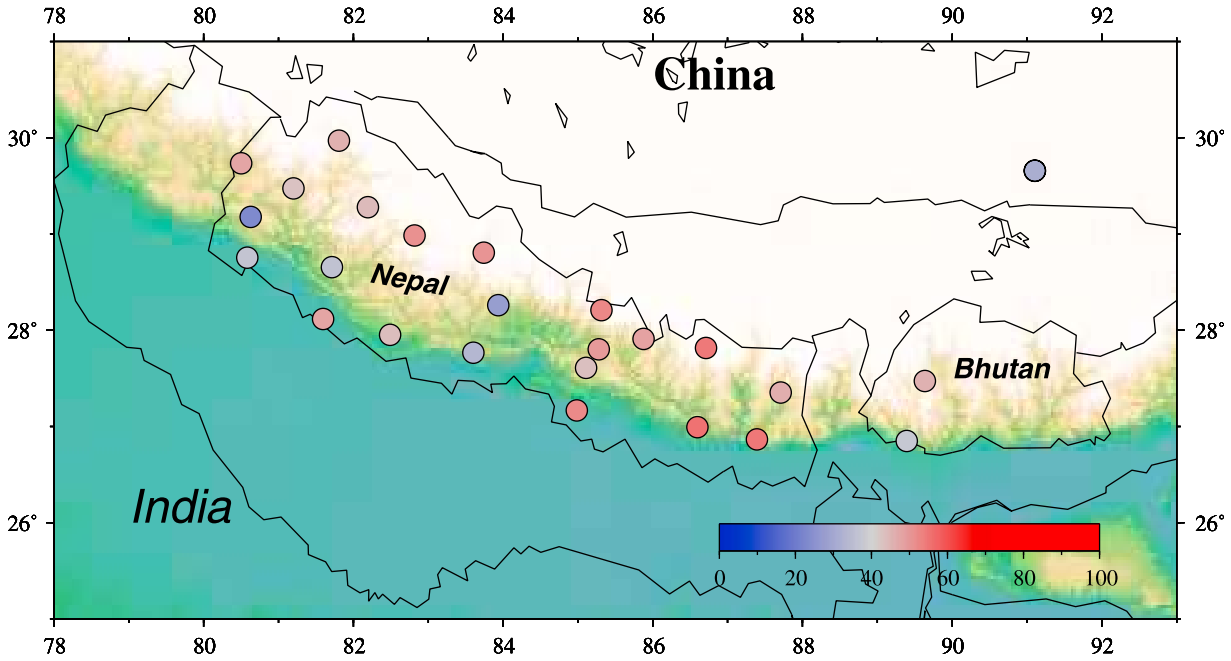

Figure 5. WRMS reductions for GPS detrended heights after removing GRACE-derived detrended displacements.

to differ due because the trends from tectonics and GIA will in general be different for these two observables.

[15] We adopted two measures to quantitatively compare the consistence between GPS and GRACE measurements. First, we remove GRACE-derived seasonal deformation from GPS observed detrended height time series, and compute the reductions of WRMS (weighted root-mean-squares) bases on the following equation [*van Dam et al.*, 2007, *Tregoning et al.*, 2009; *Tesmer et al.*, 2011].

$$WRMS_{reduction} = \frac{WRMS_{GPS} - WRMS_{GPS-GRACE}}{WRMS_{GPS}}. \quad (2)$$

We use this measure to quantitatively evaluate whether different GRACE solutions can be distinguished, and to identify which GRACE solution to employ for further discussion. We exclude the GFZ solution because of its clear outliers in 2004. For the GPS stations whose observation time is longer than 3 years, the average WRMS reductions for GRACE solutions from GRGS, CSR and JPL are 46.2%, 45.4%, 45.5%, respectively, which indicates that GRGS's GRACE solution is slightly more consistent with the GPS measurements; the difference between CSR and JPL is very small. WRMS reductions are substantial regardless of the GRACE solution used, reflecting nearly a factor of 2 reductions in WRMS. So we adopt the GRACE solution from GRGS in this paper because of its better agreements with GPS and also its better temporal resolution (10 days).

[16] WRMS reductions are plotted for each station in Figure 5. All stations show significant and consistent WRMS reduction. The WRMS reduction is significantly larger than that observed for Europe by *van Dam et al.* [2007], because of the improved GPS processing strategies adopted in this study, and also because the seasonal variations in Nepal are much larger than those for western Europe.

[17] The corrected time series include random measurement noise in addition to possible remaining systematic errors. We assess how much variation remains in the time series by comparing the WRMS of the whole time series to the short-term WRMS based on days or weeks of data. Because the time series are also expected to include colored noise [*Mao et al.*, 1999; *Williams et al.*, 2004], this provides a conservative assessment of how close to the noise floor the corrected time series are. We quantify the short-term WRMS based on a short time period (1 week, or 2 weeks). Seasonal (annual and semiannual) effects are very small during such short period, so the expected WRMS mainly reflects the basic noise level without residual seasonal effects. A typical example, site CHLM, is shown in Figure 6. The WRMS of the whole time series (shown in Figure 1) for CHLM is 8.63 mm; the WRMS of the first week and first two weeks in 2010 are 2.91 mm and 3.10 mm, respectively; so for CHLM, the WRMS from short-term noise amounts to ~33% of the WRMS for the full time series. All other stations exhibit similar results. The average percentage for the selected group (observation time span longer than 3 years) is 29.56% for 1 week period, and 31.55% for 2 week period. After removing the GRACE seasonal model, the WRMS of the whole time series is reduced to ~53.8% of the original time series, which is only ~1.75 times larger than the short-term WRMS. On other words, after correcting the seasonal effects with GRACE data, the WRMS of GPS time series is reduced from ~3 times the short-term noise level to ~1.75 times the short-term noise level. The remaining noise in the corrected time series arises from a combination of longer-term correlated noise, errors in the seasonal hydrological corrections, and interannual variations in the load. Past studies on GPS coordinate noise [*Mao et al.*, 1999; *Williams et al.*, 2004] suggest that the GPS noise is a combination of white noise plus either flicker noise or a more general power

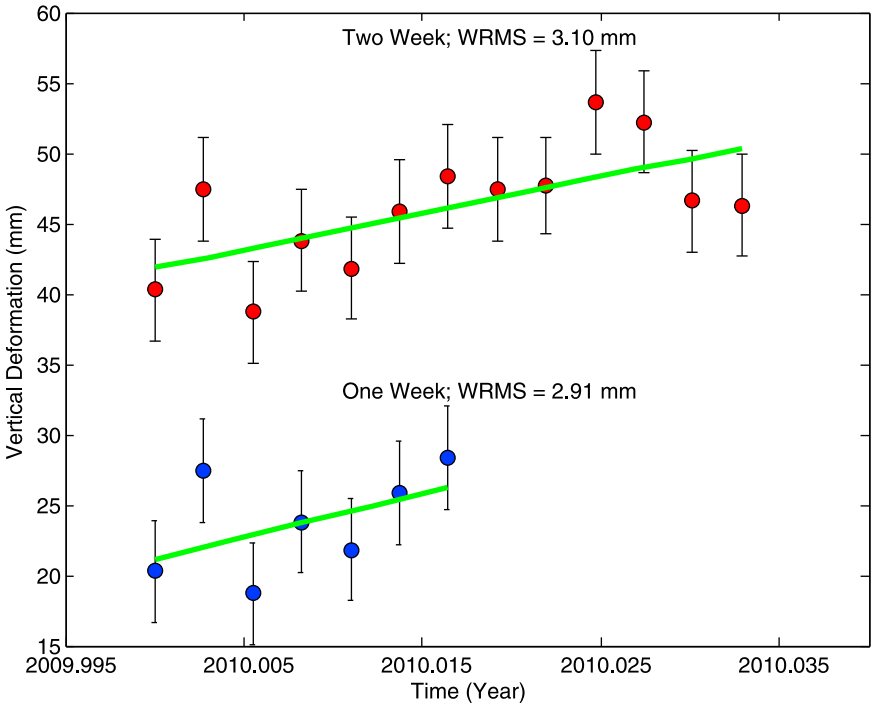

Figure 6. Short-term WRMS of station CHLM, computed based on data from the first week of 2010 (blue) and the first 2 weeks of 2010 (red), respectively.

law noise, and the coordinate uncertainty can be underestimated if the time-correlated noise is neglected.

[18] Second, we also compare the annual amplitudes for both GPS and GRACE-derived seasonal displacements (Figure 7). For this comparison, we fit both the GPS and GRACE-derived deformation time series with linear, annual, and semiannual components, and then extract and compare the amplitudes of their annual components. If the

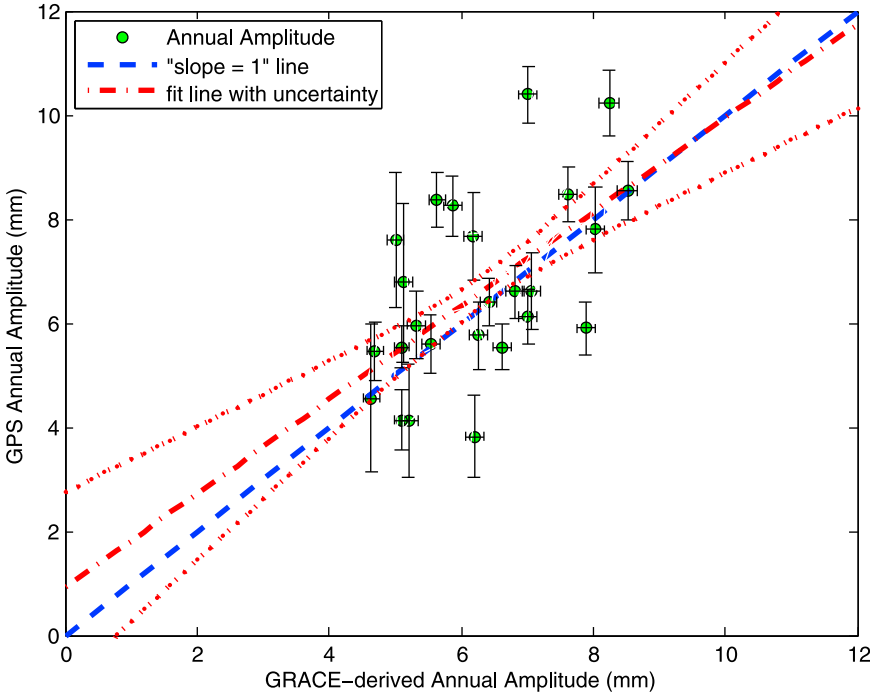

Figure 7. Comparison of annual amplitude between GPS observed heights and GRACE-derived vertical displacements. "Slope = 1" line (blue dashed) represents the ideal case in which GPS and GRACE perfectly match each other. The best fit line and its uncertainty (red dash-dot line) is derived using a weighted total least squares method with the actual measurements.

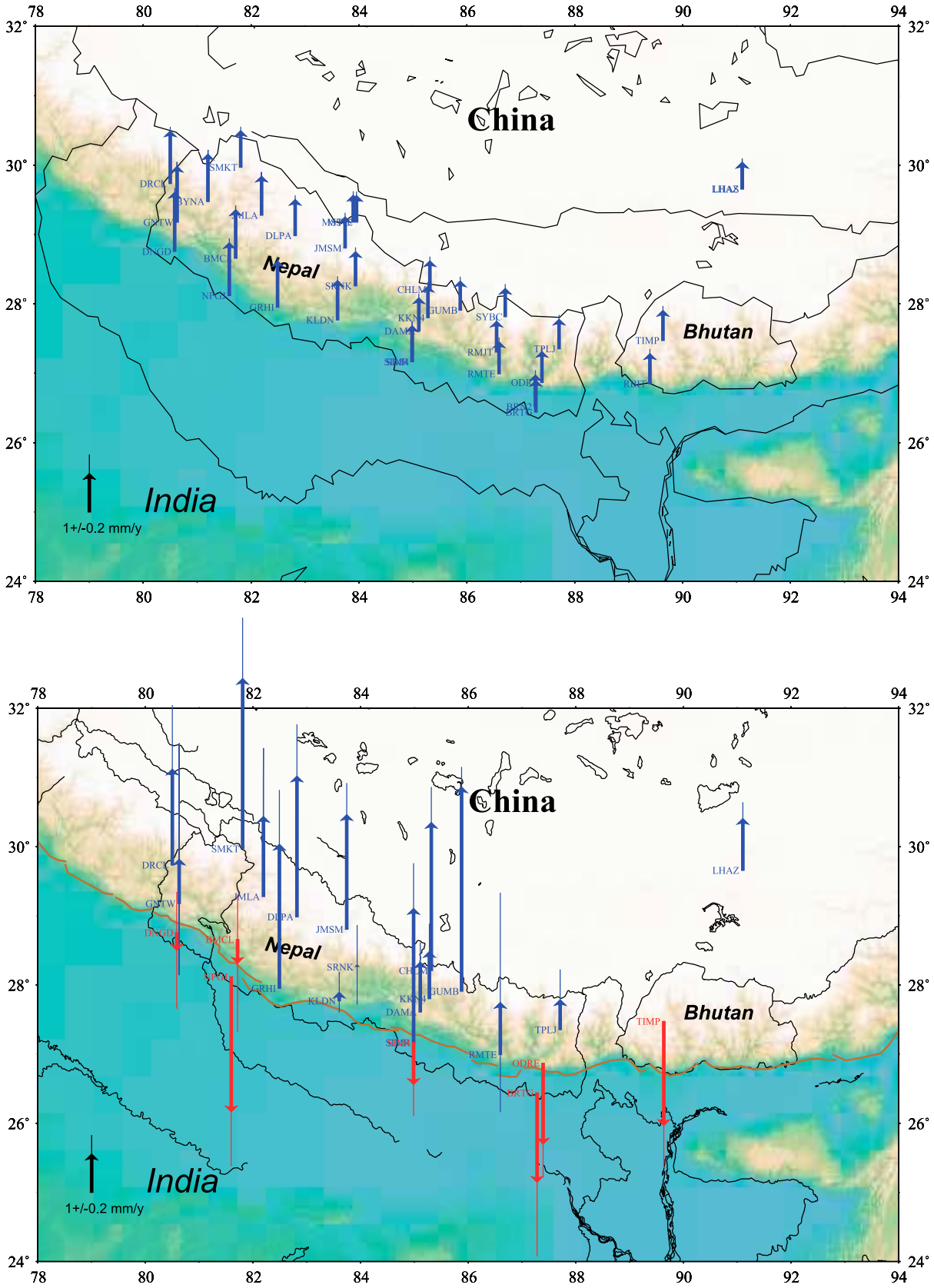

Figure 8. (top) GRACE-derived long-term uplift rates because of the mass loss in the Himalaya area. (bottom) Corrected vertical velocities after subtracting the GRACE-derived long-term uplift rate due to load changes; the brown lines indicate the frontal faults of the Main Himalayan Thrust fault system from *Lavé and Avouac* [2001].

Table 2. Parameters of the Main Himalayan Thrust Fault Model Adopted Based on Previous Studies

Model	Fault Geometry of the Creeping Zone		Velocity of Dip Slip (mm/yr)
	Depth (km)	Dip(°)	
Jouanne et al. [1999]	17	9	20.5
Jouanne et al. [2004]	19	9.5	19
Bettinelli et al. [2006]	20.9	10.3	16.3

measurements of GPS and GRACE perfectly match each other, then all the dots in Figure 7 should lie in the "slope = 1" line (blue dashed line in Figure 7). With the actual observed data and their uncertainties, we use the weighted total least squares method [*Krystek and Anton*, 2007] to derive the best fit line and its uncertainty (red dash-dot line in Figure 7), whose slope is $\sim 0.90 \pm 0.11$. Our best fit slope does not exclude a linear 1:1 relationship.

4. Long-Term Uplift Due to the Mass Loss

[19] Besides the significant seasonal variations discussed above, there is also a long-term uplift contained in GRACE-derived vertical displacement (Figure 2), which is primarily due to the mass loss in the Himalaya [*Matsuo and Heki*, 2010], and potential GIA effects. Under the influence of climate change, snow and ice in the high mountains of the Himalaya is melting rapidly. Observations from both field records [*Dyurgerov and Meier*, 2005] and satellite gravimetry (GRACE) [*Matsuo and Heki*, 2010] have confirmed this rapid ice loss. *Matsuo and Heki* [2010] reported the average ice loss rate can reach ~47 Gt/yr, equivalent to ~0.13 mm/yr global sea level rise.

[20] The earth, behaving like an elastic body, uplifts in a response to the load loss. We compute the GRACE-derived long-term uplift using the trend from the GRGS solutions for all continuous GPS sites used in this paper (Figure 8, top). The results indicate an overall uplift for the whole region, at the ~1 mm/yr level. Then we remove this cryospheric-induced uplift from GPS actual observed vertical rates to derive the corrected vertical velocities (Figure 8, bottom), which can be compared to the predictions of models that were fit to the horizontal GPS velocities. Here we assume that GIA is negligible (see section 5.2). We use CATS, a time series analysis software package [*Williams*, 2008], to estimate the velocities and their uncertainties assuming a power law noise model, and the results are included in Table 1 (column 6). The average spectral index for continuous GPS sites in Nepal is −0.42, very similar to results from other regions. *Zhang et al.* [1997] found that the mean spectral index for GPS stations in southern California is about −0.4.

5. Discussion

5.1. Tectonic Interpretation for the Corrected Vertical Rates, Assuming No GIA Effect

[21] The tectonic process in Nepal Himalaya is dynamic and dominated by the strong convergence between Indian plate and Eurasian plates. The underthrusting Indian lithosphere slides on the Main Himalayan Thrust (MHT) fault, which extends from a shallow depth under Nepal to the midcrust under southern Tibet [*Avouac*, 2003; *Nábělek et al.*, 2009]. During the interseismic period, the upper part of MHT is locked, and the lower part is creeping [*Bettinelli et al.*, 2006]. So the current observed GPS vertical rates (seasonal components removed) should be composed of both tectonic impact and the response of mass loss.

[22] We model the vertical rates for continuous GPS stations based on previous studies of interseismic slip of the MHT [*Jouanne et al.*, 1999; *Jouanne et al.*, 2004; *Bettinelli et al.*, 2006], using a two-dimensional (2-D) dislocation model [*Singh and Rani*, 1993]. The parameters of the MHT and the comparison between modeled and observed vertical rates are given in Table 2 and in Figure 9. GPS stations in Nepal with long enough observation and uncertainty of vertical rate smaller than 0.85 mm/yr are selected for this comparison. Most of the corrected vertical velocities, especially in the central part of Nepal, agree with the model predictions for interseismic strain from the MHT. However, there are several discrepancies in the western and eastern Nepal, which may reflect the lateral variation of the MHT and some local effects, such as groundwater extraction. *Rodell et al.* [2009] reports rapid groundwater extraction in India, and Nepal is also dependent on groundwater for irrigation [*Shah et al.*, 2006]. Studies indicate that withdrawal of groundwater produces localized subsidence, in which can be large relative to tectonic deformation [*Bawden et al.*, 2001; *Watson et al.*, 2002]. Besides, the lateral variations of large earthquake occurred along the Himalayan arc [*Bilham et al.*, 2001] may indicate different part of the arc is experiencing varied interseismic status.

[23] In order to verify whether the goodness of fit of the interseismic slip model is improved after correction for the uplifts due to load decrease, we compare the theoretical results from interseismic slip model of *Bettinelli et al.* [2006] and vertical rates of continuous GPS, both before and after correction. We find that the overall weighted misfit decreases by 25.0% for all the stations in Figure 9; for western and central Nepal, the model goodness of fit is improved and the misfit decreases by 11.2% and 35.1%, respectively. But the misfit in eastern Nepal actually increases by 34.4%, although this is based on only 3 sites. Because of the small number of sites, it is not clear whether the increase in misfit is significant. If it is, it might be attributed to either the inaccuracy of interseismic model, like the lateral slip variation along the arc, or the actual long-term load decrease in eastern Nepal may be not as significant as western and central parts.

5.2. GIA and Other Effects

[24] In this study, we have ignored possible effects of GIA, which can cause both gravity change and vertical motion. Whether there was a large ice sheet in the Himalaya and Tibet during the last glacier period is still debated [e.g., *Derbyshire et al.*, 1991; *Kuhle*, 1998]. *Kaufmann and Lambeck* [1997], based on a maximum large ice sheet model, predicted that present vertical and horizontal extension rates in Tibet due to GIA could reach 7 mm/yr and 2 mm/yr. *Kaufmann* [2005] presented a similar model. However, even for these models with extremely large past ice masses, the predicted effects in Nepal are small, no more than 2 mm/yr uplift rate. GIA effects are most likely smaller than predicted by these models. Field study of glacier

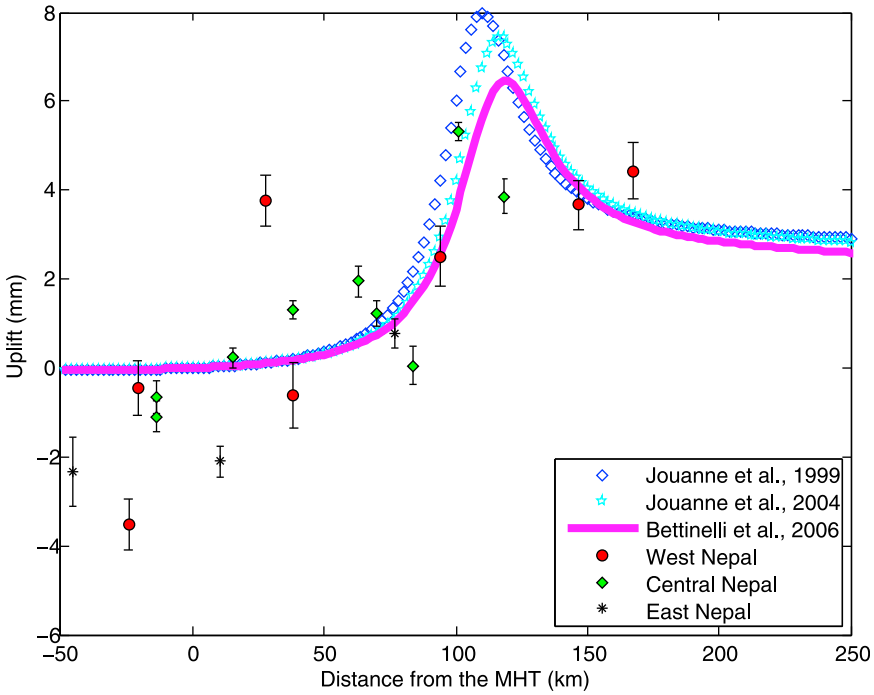

Figure 9. Comparison between GPS observed and modeled vertical rates in Nepal. Dots with error bar: corrected GPS height rates with GRACE-derived long-term uplift removed. Continuous line and blue symbols: modeled vertical rates based on previous studies that used horizontal GPS velocities.

geology [*Derbyshire et al.*, 1991] also indicates a smaller ice sheet model at the last glacier cycle, which would not produce significant present vertical displacement [*Kaufmann and Lambeck*, 1997]. In addition, GPS and absolute gravity surveys in southern and southeast Tibet [*Sun et al.*, 2009] also do not observe the uplift and gravity changes that the GIA model [*Kaufmann*, 2005] predicts. Regardless of the ice model, GIA effects on the present gravity change should not be significant in Nepal, so we neglect them for our study here.

[25] *Matsuo and Heki* [2010] argued that the tectonic uplift of Tibetan Plateau is too slow to seriously interrupt the isostatic equilibrium process, and thus would have only a small effect for the gravity change. The GRACE-derived negative gravity change (see *Matsuo and Heki* [2010, Figure 3], in terms of equivalent water height) is clearly located in the high mountain areas, and there is no obvious isostatic effect over the entire plateau. So the long-term gravity change related to tectonic isostatic equilibrium should be small relative to cryospheric effect, and probably contributes

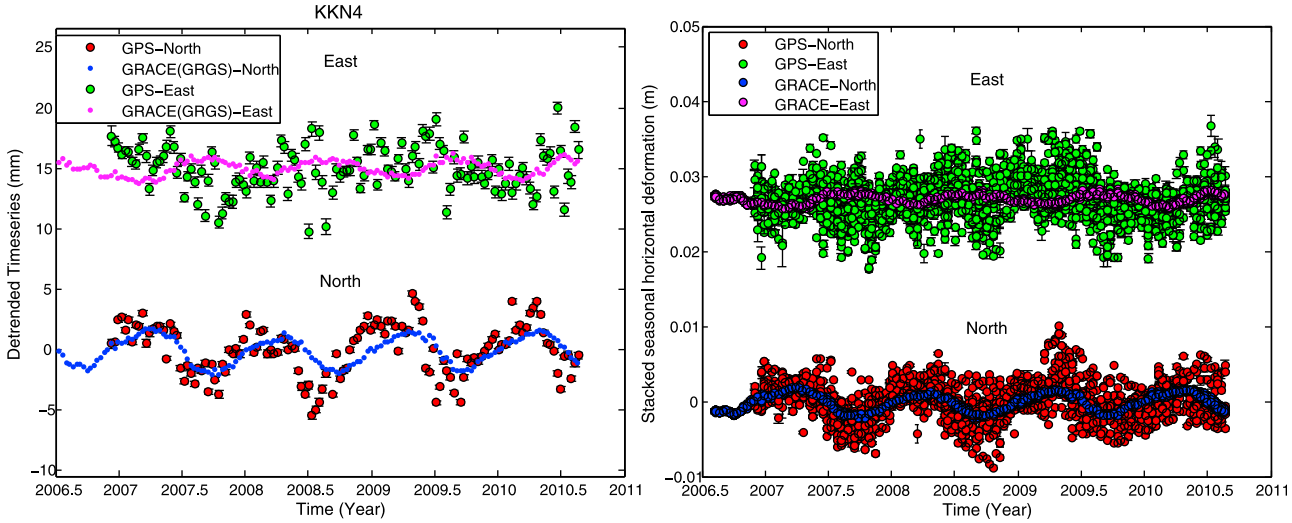

Figure 10. (left) Comparison between GPS observed and GRACE-derived horizontal seasonal (detrended) displacements for site KKN4. (right) Stacked GPS seasonal (detrended) horizontal time series and GRACE-derived seasonal horizontal time series, for the same sites as Figure 4.

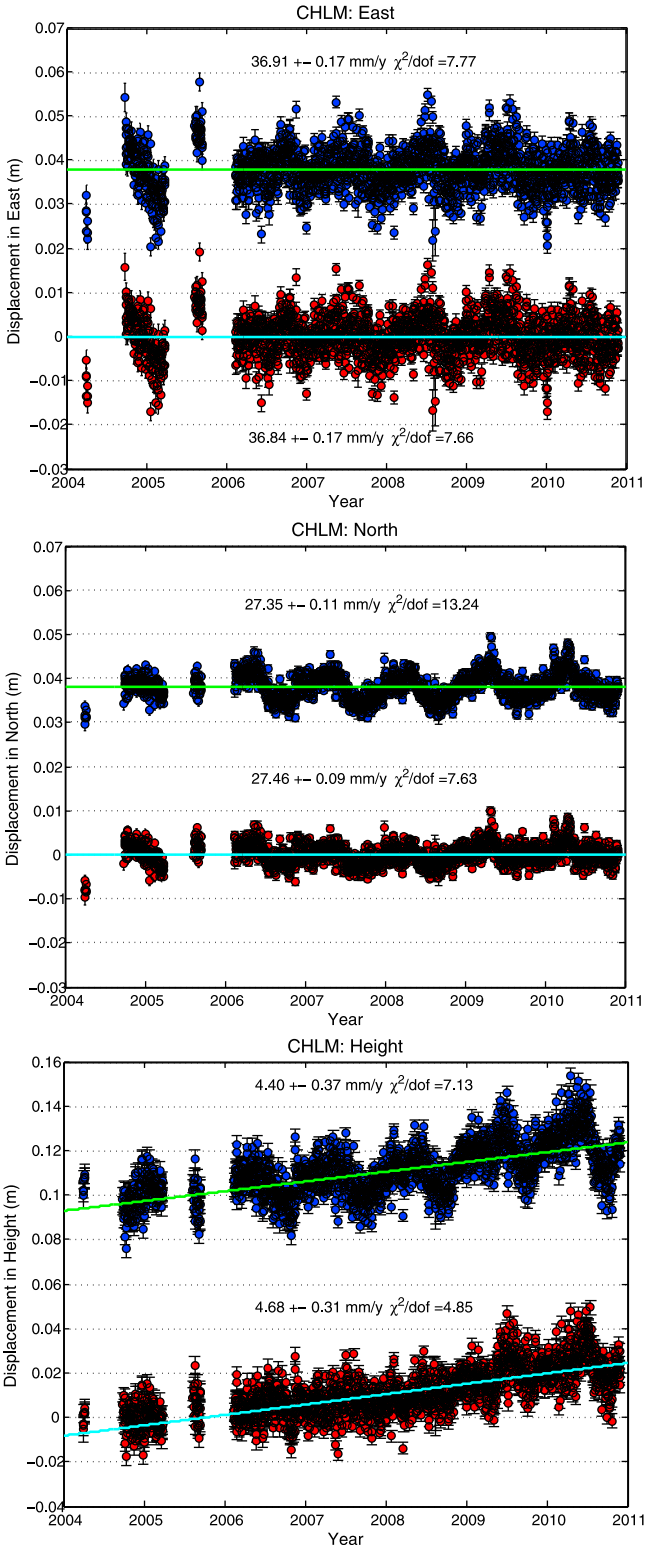

Figure 11. Comparison of linear fit between actual GPS observed time series (blue) and corrected time series (red) with seasonal effects removed, based on GRACE-derived seasonal variations. In order to better show the seasonal variations, we plot the detrended time series for the horizontal components; the horizontal velocities in ITRF2008 are given.

negligibly to the current GRACE observations. Therefore we assume the long-term gravity change revealed by GRACE data is mainly because the mass loss in the study area, and ignore the tectonic impacts on gravity change. This assumption is realistic because the cryosphere-induced gravity change in the Himalaya is much more rapid and significant.

5.3. Seasonal Variations in Horizontal Displacements

[26] *Bettinelli et al.* [2008] found seasonal variations in GPS north displacement in Nepal Himalaya, and interpreted it as due to the lithospheric response to hydrological load variation. They also demonstrated a correlation between seasonal seismicity variation and seasonal strain change produced by surface hydrological load.

[27] Here we also calculate GRACE-derived horizontal deformation, and compare it with the GPS measurements. The GRACE solution from GRGS is used here. Figure 10 shows an example (site KKN4) of the comparison between GPS observed and GRACE-derived horizontal displacements (left), and also the stacked detrended horizontal time series (right) using the same sites as Figure 4. The magnitude of GRACE seasonal variation in north is about 2∼3 times of that in east. GPS and GRACE clearly show significant and consistent seasonal variations in the north component, and the average WRMS reduction in north is ∼32.6%. The correlation between GPS and GRACE in the east component is weak, with the average WRMS reduction only ∼2.3%. This mainly reflects to the lower signal-to-noise ratio for the east component. The correlation between GPS and GRACE in the north component further confirms that the seasonal signal in GPS is caused by the hydrological load in Nepal Himalaya, which has been mainly analyzed and discussed in terms of vertical deformation in this paper.

5.4. Removing Hydrological Loading Deformation From GPS Measurements Using GRACE Data

[28] In our study, we have tried to model seasonal and long-term deformation due to hydrological effects based on GRACE observations, and compare that with the observed GPS height variation. In addition, we also attempt to remove GRACE-derived hydrological vertical rates from GPS measurements. Using this method, we manage to separate tectonic and hydrological effects, both of which contribute to the vertical velocity field. The good seasonal correlation between GPS and GRACE signals indicates that the long-term uplifts revealed by GRACE measurements are probably true and mixed in the GPS measurements.

[29] Due to a warming climate, the cryosphere is experiencing considerable mass loss globally. Large surface mass movements cause the elastic earth to deform, and this hydrology-induced deformation is superposed with other phenomenon, mainly tectonics. In this paper, we present a way to remove this hydrological effect using GRACE measurements. This method can be applied for other similar purposes. For example, seasonal variations for campaign GPS measurements usually cannot be well constrained because of their limited observations, mostly once per year. GRACE has continuous measurements since its launch in March 2002, and can provide detailed seasonal variation for gravity field and its resulting seasonal displacement due to load changes. Therefore, in order to achieve better linear

velocities for continuous or campaign GPS sites, GRACE-derived seasonal variations for vertical deformation can be used to correct seasonal influences on the GPS time series. We choose the continuous GPS station CHLM for example. In Figure 11, we compare the results for all three components: East, North, and Height. In each component, the upper time series (blue) is the original observation, and the lower (red) is the corrected time series with seasonal effects removed using GRACE-derived seasonal variations. The misfit (χ^2 divided by degrees of freedom) between data and a linear fit decreases by 32% (from 7.13 to 4.85) in height, by 42% (from 13.24 to 7.63) in north; and there is almost no decrease in east (from 7.77 to 7.66). The north component of the corrected time series shows some residual in-phase variations, which suggests that the GRACE-based load correction was too small. This could happen due to smoothing in the GRACE solution if the wavelength of the load is smaller than the smoothing length scale used in the GRACE solution. Although the example shown here is for a continuous site, the good results in height and north indicate that our method also can be employed for GPS campaign measurements. We have tested this for campaign sites with long measurement histories in the Himalaya and Tibet, and in many cases the WRMS reduction for campaign sites is $\sim$50% in height, for sites where measurements were carried out at different times of year.

6. Conclusions

[30] We combine GPS and GRACE measurements to study vertical motions in the Nepal Himalaya. Both GPS and GRACE observe strong seasonal variations. We utilize GRACE data to model the resulting vertical displacements due to the changing hydrological loads. Quantitative comparisons between the observed GPS seasonal vertical deformation and GRACE-derived seasonal deformation demonstrate that a consistent physical mechanism is responsible for the correlation between these two kinds of geodetic measurements. Besides the significant seasonal signal, GRACE also exhibits a long-term mass loss in this region, which is principally due to the melting ice and snow in high mountains of the Himalaya. We calculate the consequent uplift caused by the load decrease, and remove this hydrological effect from observed GPS vertical rates. The residual vertical rates are mainly dominated by tectonic deformation due to the earthquake cycle in the thrusting. We then employ a 2-D dislocation model to compute the tectonic vertical rates based on previous studies; those studies estimated fault models from the GPS horizontal velocities. Comparison between observed and modeled vertical rates suggests that the interseismic slip of MHT is able to explain the most of the vertical motion of most GPS stations, although the whole arc shows some lateral variations. Correction for the long-term uplift predicted by the GRACE data improves the agreement between GPS vertical rates and the models based on horizontal data. The GPS vertical velocities are still too noisy to discriminate between the different horizontal slip models, but they may contribute to the estimation of models based on 3D velocities once loading effects are removed.

[31] **Acknowledgments.** The authors gratefully appreciate Jean-Philippe Avouac and his group at Caltech Tectonics Observatory for establishing and maintaining the GPS stations in Nepal, and for making the data available to the public. The two stations in Bhutan were set up and operated by the Geological Survey of Bhutan (Dowchu Dukpa) and the Royal Bhutan Institute of Technology (G. Prasad Babu) in collaboration with Roger Bilham of the University of Colorado. This study could not have been done without their work and their generous sharing of the data with the public. We also thank the GRGS, CSR, GFZ, and JPL teams for their online accessible GRACE solutions. Kosuke Heki and an anonymous reviewer provided helpful comments and suggestions that improve the manuscript. Discussions with Anthony Arendt and Ronni Grapenthin (Geophysical Institute, UAF), Lin Liu (Stanford University) and Jin Li (Shanghai Astronomical Observatory) also help this study. This work is supported by NSF grant EAR-0911677.

References

Avouac, J. P. (2003), Mountain building, erosion, and the seismic cycle in the Nepal Himalaya, *Adv. Geophys.*, *46*, 1–80.

Bawden, G. W., W. Thatcher, R. S. Stein, C. Wicks, K. Hudnut, and G. Peltzer (2001), Tectonic contraction across Los Angeles after removal of groundwater pumping effects, *Nature*, *412*, 812–815, doi:10.1038/35090558.

Bettinelli, P., J.-P. Avouac, M. Flouzat, F. Jouanne, L. Bollinger, P. Wills, and G. R. Chitrakar (2006), Plate motion of India and interseismic strain in the Nepal Himalaya from GPS and DORIS measurements, *J. Geod.*, *80*, 567–589, doi:10.1007/s00190-006-0030-3.

Bettinelli, P., J.-P. Avouac, M. Flouzat, L. Bollinger, G. Ramillien, S. Rajaure, and S. Sapkota (2008), Seasonal variations of seismicity and geodetic strain in the Himalaya induced by surface hydrology, *Earth Planet. Sci. Lett.*, *266*, 332–344, doi:10.1016/j.epsl.2007.11.021.

Bilham, R., V. K. Gaur, and P. Molnar (2001), Himalayan seismic hazard, *Science*, *293*, 1442–1444, doi:10.1126/science.1062584.

Blewitt, G., D. Lavallée, P. Clarke, and K. Nurudinov (2001), A new global model of Earth deformation: Seasonal cycle detected, *Science*, *294*, 2342–2345, doi:10.1126/science.1065328.

Boehm, J., A. Niell, P. Tregoning, and H. Schuh (2006), Global Mapping Function (GMF): A new empirical mapping function based on numerical weather model data, *Geophys. Res. Lett.*, *33*, L07304, doi:10.1029/2005GL025546.

Boehm, J., R. Heinkelmann, and H. Schuh (2007), Short note: A global model of pressure and temperature for geodetic applications, *J. Geod.*, *81*, 679–683, doi:10.1007/s00190-007-0135-3.

Bruinsma, S., J. Lemoine, R. Biancale, and N. Vales (2010), CNES/GRGS 10-day gravity field models (release 2) and their evaluation, *Adv. Space Res.*, *45*, 587–601, doi:10.1016/j.asr.2009.10.012.

Chen, J. L., C. R. Wilson, and B. D. Tapley (2006), Satellite gravity measurements confirm accelerated melting of Greenland Ice Sheet, *Science*, *313*, 1958–1960, doi:10.1126/science.1129007.

Cheng, M., and B. D. Tapley (2004), Variations in the Earth's oblateness during the past 28 years, *J. Geophys. Res.*, *109*, B09402, doi:10.1029/2004JB003028.

Derbyshire, E., Y. Shi, J. Li, B. Zheng, S. Li, and J. Wang (1991), Quaternary glaciation of Tibet: The geological evidence, *Quat. Sci. Rev.*, *10*, 485–510, doi:10.1016/0277-3791(91)90042-S.

Dong, D., P. Fang, Y. Bock, M. K. Cheng, and S. Miyazaki (2002), Anatomy of apparent seasonal variations from GPS-derived site position time series, *J. Geophys. Res.*, *107*(B4), 2075, doi:10.1029/2001JB000573.

Dyurgerov, M., and M. F. Meier (2005), Glaciers and the changing earth system: A 2004 snapshot, *Rep. INSTAAR/OP-58*, pp. 118, Inst. of Arctic and Alpine Res., Univ. of Colo., Boulder.

Farrell, W. E. (1972), Deformation of the Earth by surface loads, *Rev. Geophys.*, *10*, 761–797, doi:10.1029/RG010i003p00761.

Fu, Y., J. T. Freymueller, and T. van Dam (2012), The effect of using inconsistent ocean tidal loading models on GPS coordinate solutions, *J. Geod.*, doi:10.1007/s00190-011-0528-1, in press.

Grapenthin, R., F. Sigmundsson, H. Geirsson, T. Árnadóttir, and V. Pinel (2006), Icelandic rhythmics: Annual modulation of land elevation and plate spreading by snow load, *Geophys. Res. Lett.*, *33*, L24305, doi:10.1029/2006GL028081.

Heki, K. (2001), Seasonal modulation of interseismic strain buildup in north-eastern Japan driven by snow loads, *Science*, *293*, 89–92, doi:10.1126/science.1061056.

Jouanne, F., et al. (1999), Oblique convergence in Himalaya of western Nepal deduced from preliminary results of GPS measurements, *Geophys. Res. Lett.*, *26*, 1933–1936, doi:10.1029/1999GL900416.

Jouanne, F., J. L. Mugnier, J. F. Gamond, P. Le Fort, M. R. Pandey, L. Bollinger, M. Flouzat, and J. P. Avouac (2004), Current shortening across the Himalayas of Nepal, *Geophys. J. Int.*, *157*, 1–14, doi:10.1111/j.1365-246X.2004.02180.x.

Kaufmann, G. (2005), Geodetic signatures of a Late Pleistocene Tibetan ice sheet, *J. Geodyn.*, *39*, 111–125.

Kaufmann, G., and K. Lambeck (1997), Implications of Late Pleistocene glaciation of the Tibetan Plateau for present-day uplift rates and gravity anomalies, *Quat. Res.*, *48*, 267–279, doi:10.1006/qres.1997.1924.

Khan, S. A., J. Wahr, M. Bevis, I. Velicogna, and E. Kendrick (2010), Spread of ice mass loss into northwest Greenland observed by GRACE and GPS, *Geophys. Res. Lett.*, *37*, L06501, doi:10.1029/2010GL042460.

Krystek, M., and M. Anton (2007), A weighted total least-squares algorithm for fitting a straight line, *Meas. Sci. Technol.*, *18*, 3438–3442, doi:10.1088/0957-0233/18/11/025.

Kuhle, M. (1998), Reconstruction of the 2.4 million km^2 late Pleistocene ice sheet on the Tibetan Plateau and its impact on the global climate, *Quat. Int.*, *45–46*, 71–108, doi:10.1016/S1040-6182(97)00008-6.

Kusche, J., and E. J. O. Schrama (2005), Surface mass redistribution inversion from global GPS deformation and Gravity Recovery and Climate Experiment (GRACE) gravity data, *J. Geophys. Res.*, *110*, B09409, doi:10.1029/2004JB003556.

Lavé, J., and J. P. Avouac (2001), Fluvial incision and tectonic uplift across the Himalayas of central Nepal, *J. Geophys. Res.*, *106*, 26,561–26,591, doi:10.1029/2001JB000359.

Luthcke, S. B., A. A. Arendt, D. D. Rowlands, J. J. McCarthy, and C. F. Larsen (2008), Recent glacier mass changes in the Gulf of Alaska region from GRACE mascon solutions, *J. Glaciol.*, *54*, 767–777, doi:10.3189/002214308787779933.

Mao, A., C. G. A. Harrison, and T. H. Dixon (1999), Noise in GPS coordinate time series, *J. Geophys. Res.*, *104*, 2797–2816, doi:10.1029/1998JB900033.

Matsuo, K., and K. Heki (2010), Time-variable ice loss in Asian high mountains from satellite gravimetry, *Earth Planet. Sci. Lett.*, *290*, 30–36, doi:10.1016/j.epsl.2009.11.053.

Molnar, P., and P. Tapponnier (1975), Cenozoic tectonics of Asia: Effects of a continental collision, *Science*, *189*, 419–426, doi:10.1126/science.189.4201.419.

Nábělek, J., et al. (2009), Underplating in the Himalaya-Tibet collision zone revealed by the Hi-CLIMB experiment, *Science*, *325*, 1371–1374, doi:10.1126/science.1167719.

Rodell, M., I. Velicogna, and J. S. Famiglietti (2009), Satellite-based estimates of groundwater depletion in India, *Nature*, *460*, 999–1002, doi:10.1038/nature08238.

Schmid, R., P. Steigenberger, G. Gendt, M. Ge, and M. Rothacher (2007), Generation of a consistent absolute phase center correction model for GPS receiver and satellite antennas, *J. Geod.*, *81*, 781–798, doi:10.1007/s00190-007-0148-y.

Shah, T., O. P. Singh, and A. Mukherji (2006), Some aspects of South Asia's groundwater irrigation economy: Analyses from a survey in India, Pakistan, Nepal Terai and Bangladesh, *Hydrogeol. J.*, *14*, 286–309, doi:10.1007/s10040-005-0004-1.

Singh, S. J., and S. Rani (1993), Crustal deformation associated with two dimensional thrust faulting, *J. Phys. Earth*, *41*, 87–101, doi:10.4294/jpe1952.41.87.

Steckler, M. S., S. L. Nooner, S. H. Akhter, S. K. Chowdhury, S. Bettadpur, L. Seeber, and M. G. Kogan (2010), Modeling Earth deformation from monsoonal flooding in Bangladesh using hydrographic, GPS, and Gravity Recovery and Climate Experiment (GRACE) data, *J. Geophys. Res.*, *115*, B08407, doi:10.1029/2009JB007018.

Sun, W., Q. Wang, H. Li, Y. Wang, S. Okubo, D. Shao, D. Liu, and G. Fu (2009), Gravity and GPS measurements reveal mass loss beneath the Tibetan Plateau: Geodetic evidence of increasing crustal thickness, *Geophys. Res. Lett.*, *36*, L02303, doi:10.1029/2008GL036512.

Swenson, S., D. Chambers, and J. Wahr (2008), Estimating geocenter variations from a combination of GRACE and ocean model output, *J. Geophys. Res.*, *113*, B08410, doi:10.1029/2007JB005338.

Tesmer, V., P. Steigenberger, T. van Dam, and T. Mayer-Gürr (2011), Vertical deformations from homogeneously processed GRACE and global GPS long-term series, *J. Geod.*, *85*, 291–310, doi:10.1007/s00190-010-0437-8.

Thomas, J., and S. C. Rai (2005), An overview of glaciers, glacier retreat, and subsequent impacts in Nepal, India, and China, report, 70 pp., WWF Nepal Programme, Kathmandu.

Tregoning, P., C. Watson, G. Ramillien, H. McQueen, and J. Zhang (2009), Detecting hydrologic deformation using GRACE and GPS, *Geophys. Res. Lett.*, *36*, L15401, doi:10.1029/2009GL038718.

van Dam, T., J. Wahr, and D. Lavallée (2007), A comparison of annual vertical crustal displacements from GPS and Gravity Recovery and Climate Experiment (GRACE) over Europe, *J. Geophys. Res.*, *112*, B03404, doi:10.1029/2006JB004335.

Wahr, J., M. Molenaar, and F. Bryan (1998), Time variability of the Earth's gravity field: Hydrological and oceanic effects and their possible detection using GRACE, *J. Geophys. Res.*, *103*, 30,205–30,229, doi:10.1029/98JB02844.

Watson, K. M., Y. Bock, and D. T. Sandwell (2002), Satellite Interferometric observations of displacements associated with seasonal groundwater in the Los Angeles basin, *J. Geophys. Res.*, *107*(B4), 2074, doi:10.1029/2001JB000470.

Williams, S. D. P. (2008), CATS: GPS coordinate time series analysis software, *GPS Solut.*, *12*, 147–153, doi:10.1007/s10291-007-0086-4.

Williams, S. D. P., Y. Bock, P. Fang, P. Jamason, R. M. Nikolaidis, L. Prawirodirdjo, M. Miller, and D. J. Johnson (2004), Error analysis of continuous GPS position time series, *J. Geophys. Res.*, *109*, B03412, doi:10.1029/2003JB002741.

Wu, X., M. B. Heflin, E. R. Ivins, D. F. Argus, and F. H. Webb (2003), Large-scale global surface mass variations inferred from GPS measurements of load-induced deformation, *Geophys. Res. Lett.*, *30*(14), 1742, doi:10.1029/2003GL017546.

Zhang, J., Y. Bock, H. Johnson, P. Fang, S. Williams, J. Genrich, S. Wdowinski, and J. Behr (1997), Southern California Permanent GPS Geodetic Array: Error analysis of daily position estimates and site velocities, *J. Geophys. Res.*, *102*, 18,035–18,055, doi:10.1029/97JB01380.

J. T. Freymueller and Y. Fu, Geophysical Institute, University of Alaska Fairbanks, Fairbanks, AK 99775-7320, USA. (jeff.freymueller@gi.alaska.edu; yuning@gi.alaska.edu)